Analysis of the Surface Chemical Composition and Morphological Structure of Vapor-Sensing Gold−Fluoropolymer Nanocomposites

N. Cioffi,[†] I. Losito,[†,||] L. Torsi,*[,†,||] I. Farella,[‡] A. Valentini,[‡] L. Sabbatini,[†,||] P. G. Zambonin,[†,||] and T. Bleve-Zacheo[§]

Dipartimento di Chimica, Università degli Studi di Bari, via Orabona 4, I-70126 Bari, Italy, INFM-Unità di Bari, Dipartimento Interateneo di Fisica, via Amendola 173, I-70126 Bari, Italy, Istituto di Nematologia Agraria Applicata ai Vegetali, Consiglio Nazionale delle Ricerche, I-70126 Bari, Italy, and Center of Innovative Technologies for Signal Detection and Processing, University of Bari, Italy

Received July 20, 2001. Revised Manuscript Received October 22, 2001

A systematic spectroscopic and morphological characterization of gold−fluoropolymer (CF_x(Au)) nanocomposites, deposited by ion beam cosputtering, is presented. These composites are technologically relevant, since they exhibit vapor-sensing properties based on swelling phenomena. Analysis by X-ray photoelectron spectroscopy (XPS) allows us to assess that gold codeposition induces a progressive defluorination of the polymeric chains, leading to a significant increase of the polymer chains' branching and of the concentration of unsaturated fluorinated carbons. The presence of a fluoride peak in the F 1s spectrum proves the formation of polar gold fluorides. Transmission electron microscopy reveals the presence of in-plane homogeneously distributed nanosized gold domains, while angle-resolved X-ray photoelectron spectroscopy indicates a nonhomogeneous in-depth distribution of the gold particles, with the outer surface being less rich in nanoparticles. Results derived from the analytical characterization allow a deeper understanding of the swelling phenomena involved in the sensing processes.

Introduction

The controlled incorporation of metal nanoclusters into polymeric matrixes is a research topic of considerable interest because the metallic species can dramatically influence the chemical and physical properties of the resultant composite material. Many efforts have been expended in the past decade in order to elucidate the structure and properties of fuoropolymers modified by deposition of either thin metallic layers[1−7] or nanosized clusters.[8−16] The high scientific and industrial interest in metal−Teflon composites is due to the wide range of applications that these materials have, for instance in microelectronics,[17] as biocompatible materials,[18] and in nonlinear optics[19] or optical recordings,[8−10] just to cite a few. Gold−fluoropolymer (CF_x(Au)) nanostructured composites have been successfully fabricated employing technologies such as plasma deposition[15] and ion cosputtering.[20,21] The latter is particularly interesting being a cost-effective and environmental friendly technology, allowing also a higher degree of control over important deposition parameters such as the sputtering energy and the metal loading. Moreover, ion cosputtered CF_x(Au) films have been recently employed as active layers in gas-sensing devices based on swelling phenomena.[20,21]

* Corresponding author. Phone: +39 080 5442019. Fax: + 39 080 5442026. E-mail: torsi@chimica.uniba.it.
[†] Università degli Studi di Bari.
[‡] INFM-Unità di Bari.
[§] Consiglio Nazionale delle Ricerche.
[||] C.I.T.S.D.P., University of Bari.

(1) Roy, R. A.; Messier, R.; Krishnaswamy, S. V. *Thin Solid Films* **1983**, *109*, 27.
(2) Shi, M. K.; Lamontagne, B.; Selmani, A.; Martinu, L. *J. Vac. Sci. Technol. A* **1994**, *12*, 44.
(3) Shi, M. K.; Lamontagne, B.; Selmani, A.; Martinu, L.; Sacher, E.; Wertheimer, M. R.; Yelon, A. *J. Vac. Technol. A* **1994**, *12*, 807.
(4) Kinbara, A.; Kikuchi, A.; Baba, S.; Abe, T. *J. Adhesion Sci. Technol.* **1993**, *7*, 457.
(5) Kim, Y. K.; Chang, C. A.; Schrott, A. G. *J. Appl. Phys.* **1990**, *67*, 251.
(6) Meyer, H.; Schulz, R.; Suhr, H.; Haag, C.; Horn, K.; Bradshaw, A. M. *Met. Plast.* **1992**, *2*, 121.
(7) Laetsch, S.; Hiraoka, H.; Bargon, J. *Mater. Res. Soc. Symp. Proc.* **1995**, *385*, 239.
(8) Goto, A. *Jpn. Kokai Tokkyo Koho* **1988**, 7 pp, patent.
(9) Gritsenko, K. P. *Proc. SPIE-Int. Soc. Opt. Eng.* **1998**, *3347*, 165.
(10) Ueda, Y.; Yashiro, T. *Jpn. Kokai Tokkyo Koho* **1992**, 3 pp, patent.
(11) Martinu, L.; Biederman, H. *Vacuum* **1986**, *36*, 477.
(12) Kay, E.; Hecq, M. *J. Appl. Phys.* **1984**, *55*, 370.
(13) Biederman, H. *J. Vac. Sci. Technol. A* **2000**, *18*, 1642 and references therein cited.
(14) Nosaka, T.; Ogawa, S.; Takiguchi, K.; Yoshitake, M.; Okamoto, A.; Fuji, M. *Shinku* **1989**, *32*, 319.
(15) Perrin, J.; Despax, B.; Kay, E. *Phys. Rev. B: Condens. Matter* **1985**, *32*, 719 and references therein cited.
(16) Laurent, C.; Kay, E. *Z. Phys. D: At., Mol. Clusters* **1989**, *12*, 465.
(17) Wu, P. K. *Mater. Res. Soc. Symp. Proc.* **1995**, *385*, 79 and references therein cited.
(18) McLaughlin, J. A.; Macken, D.; Meenan, B. J.; McAdams, E. T.; Maguire, P. D. *Key Eng. Mater.* **1995**, *99*, 331.
(19) Dalacu, D.; Brown, A. P.; Klemberg-Sapieha, J. E.; Martinu, L.; Wertheimer, M. R.; Najafi, S. I.; Andrews, M. A. *Mater. Res. Soc. Symp. Proc.* **1999**, *544*, 167.
(20) D'Addabbo, A.; Valentini, A.; Convertino, A. *J. Appl. Phys.* **2000**, *87*, 2039.
(21) Bassi, A.; Valentini, A.; Convertino, A. *Appl. Phys. A: Mater. Sci. Process.* **2000**, *71*, 109.

10.1021/cm0111940 CCC: $22.00
Published on Web 01/26/2002

Table 1. Volume Fraction and Density for Different Composites; Ion Beam Energy, Current, and Growth Rates for Both CF_x and Au

		CF_x			Au		
φ	density (g/cm^3)	beam energy (eV)	beam current (mA)	growth rate (nm/s)	beam energy (eV)	beam current (mA)	growth rate (nm/s)
0.00	2.10	750	50	0.14			
0.05	2.96				300	25	0.01
0.10	3.82				400	35	0.02
0.15	4.68				470	50	0.03
0.30	7.26				615	58	0.04

The aim of the present study is to assess the surface chemical composition and morphological structure of ion cosputtered Teflon-like−gold nanostructured materials, to provide the basis for a deeper understanding of the interaction mechanisms involved in the vapor-sensing process and for a better definition of structure/device-performance correlations.

Experimental Section

Sample Deposition. CF_x(Au) samples have been deposited on silicon substrates by cosputtering a Teflon target and a gold one with Ar^+ ion beams at room temperature and at a pressure of about 10^{-4} mbar. Details on the ion-beam sputtering (IBS) deposition technique and apparatus have been reported elsewhere.[22] Each component growth rate (r) at different values of the ion beam energy and current was evaluated in situ by means of a quartz oscillator balance placed near the substrate.[23] The metal volume fraction (φ) is derived from the relation

$$\varphi = (r_{Au}/r_{CF_x})/[1 + (r_{Au}/r_{CF_x})]$$

where r_{Au} and r_{CF_x} are the growth rates of gold and CF_x, respectively. By suitably choosing the ion beam parameters (energy and current), and hence the growth rate ratio, it was possible to synthesize gold−fluorocarbon composite films with gold volume fractions ranging in the interval $0 \le \varphi \le 0.30$. The thickness of the composites was 200 nm, unless otherwise stated. The composite density was calculated as the φ-weighted mean of the density values relevant to pure bulk materials. The density of standard Teflon (ρ_{Tefl}) was used as an estimation of that of the fluoropolymer. Volume fractions, growth rates, densities, and sputtering parameters of composite films are summarized in Table 1.

In the calculation of the bulk atomic percentages corresponding to a certain value of φ, the following equations were used to obtain the Au, C, and F number of atoms (N):

$$N_{Au} = \frac{\varphi \rho_{Au} V_{tot}}{M_{Au}}; \quad N_C = \frac{(1-\varphi)\rho_{Tefl} V_{tot}}{M_C + xM_F}; \quad N_F = xN_C$$

where V_{tot} is the volume of the composite, M is the atomic weight, x is the F/C ratio obtained by the XPS analysis, and ρ_{Au} is the density of bulk Au.

Vapor-Sensing Measurements. The nanocomposite swelling was evaluated by introducing acetone vapors into a low vacuum chamber. The vapor pressure (in the range 10^{-2} to 20 mbar) was evaluated by means of a Pirani gauge, and the film thickness was measured with a single wavelength Jobin Yvon-Sofie ellipsometer operating at 632.8 nm.

Morphological Characterization. Electron beam transparent 10 nm thick films for TEM characterization were deposited on 400 mesh *Formwar*-coated nickel grids. All the samples were observed at 100 kV under a PHILIPS 400T TEM. Size determination of the gold cluster cores was manually performed for more than 600 particles, selected in 4−6 different regions of the micrographs. The surface morphology of the composite films was studied with a Danish Micro Engineering dualscope atomic force microscope (AFM), operated in tapping mode.

Surface Characterization. XPS measurements were performed using a Leybold LHS10 spectrometer equipped with an unmonochromatized Al Kα source. Survey spectra were acquired in fixed retarding ratio mode (retarding ratio = 3), and high-resolution spectra (for F 1s, C 1s, Au 4f, and O 1s regions) were recorded in fixed analyzer transmission mode, with a pass energy of 50 eV. Calibration of the spectra was performed by taking the CF_2 component of the C 1s electron peak (Binding Energy, BE = 291.8 eV) as internal reference.[3] Data analysis was performed as reported in ref 24. The same half width at half maximum (HWHM) value was employed for the curve-fitting of peaks belonging to the same high-resolution spectrum. C 1s and F 1s HWHM values were respectively chosen in the 0.8−1.05 eV and 1.1−1.25 eV ranges, as a function of the sample charging. The uncertainty reported for the binding energy value of each fitting peak is relevant to sample-to-sample variations, since the errors associated with each fitting procedure are always much smaller. The smallest error was 0.1 eV, which is the energy step employed for data acquisition. The error associated with each fitting peak intensity derives from the curve-fitting.

Sample Degradation under X-rays. X-ray-promoted fluorine loss from Teflon-like materials is a well-known phenomenon[2,25] that has been taken into consideration as a possible source of artifacts. Upon exposure to X-rays, the intensity of the F 1s signal, normalized by its maximum value recorded after 3 min of irradiation, decreased linearly, in the 3′−180′ time range, with a slope of -8.0×10^{-4} min^{-1} (R^2= 0.994). The intensity of the other signals did not change in the same time interval, which is much larger than the overall analysis duration (typically 60′). Accordingly, the acquisition order of the spectral regions was chosen as follows: F 1s, C 1s, Au 4f, O 1s, and survey spectrum. Because of their high intensity, the F 1s and C 1s signals required only a few scans and, consequently, a few minutes of exposure to X-rays (1−3′ in the case of F 1s, 10′−15′ for C 1s). The number of scans was reduced to the minimum also for the Au 4f region. Moreover, replicate acquisitions of the Au 4f signal at different exposure times did not evidence changes even in its shape. On the basis of these considerations, artifacts deriving from fluorine loss were excluded.

Results and Discussion

Vapor-Sensing Responses. When exposed to organic vapors, CF_x(Au) films undergo swelling processes that depend on the gold loading in the material.[20−21] The structural modifications induced by swelling can be used to reveal a gaseous analyte by means of various approaches. Vapor-sensing experiments can be performed through the swelling evaluation by a direct ellipsometric measurement of the material thickness changes. Moreover, swelling causes the modification of fundamental properties, such as conductivity, that can be used in conventional (i.e. conductivity-variation based) gas-sensing devices.[20] On the basis of the former approach, the vapor-sensing−swelling behavior of CF_x(Au) films having a gold volume fraction (φ) of 0.05−0.15 is reported in Figure 1, where it is compared with the response of a CF_x ($\varphi = 0$) film. As is evident from the figure, upon exposure to low pressures of acetone

(22) Quaranta, F.; Valentini, A.; Rizzi, F. R.; Casamassima, G. *J. Appl. Phys.* **1993,** *74*, 244.
(23) Quaranta, F.; Valentini, A.; Favia, P.; Lamendola, R.; D′Agostino, R. *Appl. Phys. Lett.* **1993,** *63*, 10.
(24) Malitesta, C.; Losito, I.; Sabbatini, L.; Zambonin, P. G. *J. Electron Spectrosc. Relat. Phenom.* **1995**, *76*, 629.
(25) Strohmeier, B. R. *Appl. Surf. Sci.* **1991**, *47*, 225.

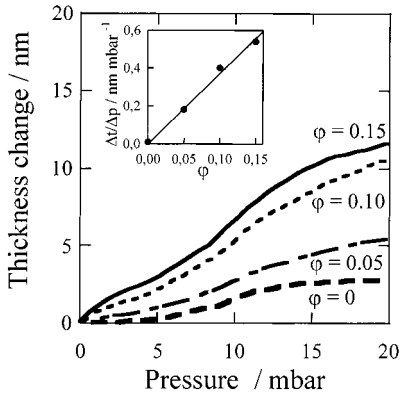

Figure 1. Gas-sensing properties of CF_x ($\varphi = 0$) and CF_x(Au) ($\varphi = 0.05-0.15$) films: thickness change vs acetone vapor pressure. In the inset: dependence of the material swelling sensitivity (thickness change per acetone pressure unit) toward acetone as a function of the gold loading.

vapors (up to 20 mbar), the films undergo thickness variations that are almost linear with the acetone pressure. Furthermore, the swelling sensitivity of CF_x(Au) composites toward acetone is higher than that of the Teflon-like film, and it is proportional to the gold amount in the material, φ being a key parameter to tune the sensor response (see the inset of Figure 1). Interestingly, preliminary measurements show a correlation between the thickness variation and the polarity of the target molecule. As a matter of fact, CCl_4 vapors generate a much lower degree of swelling than acetone or 2-propanol. Discussion on this experimental evidence is reported later in the text.

Composites' Morphology. In Figure 2 TEM images relevant to CF_x(Au) composite thin films having different gold contents are shown; the composite films look homogeneous over a wide spatial range, while the morphology of their inorganic domains is a function of φ. The average diameter increases, and the numeric density of the gold nanoparticles (Au-NPs) decreases with φ (see Table 2). For φ values close to the percolation limit, aggregation of the Au-NPs occurs, leading to larger island-shaped clusters. AFM investigation of the CF_x(Au) films showed that the sample surface is particularly smooth (see Figure 3); the largest holes are few nanometers wide and deep, while the average sample roughness, measured over the entire image, is 0.87 nm. The small craters on the surface could be due either to natural roughness of the samples or to the impact of sputtered Au-NPs during the last phases of the deposition.

XPS Surface Characterization. *Conventional and Angle-Resolved Elemental Analysis.* The surface atomic percentage and fluorine/carbon ratio variation upon gold loading are reported in Figure 4; the following three evidences can be outlined: (i) the gold surface concentration is systematically lower than that of the bulk; (ii) the oxygen concentration in the composites, although always lower than 1%, increases with the gold loading; (iii) the F/C ratio decreases as φ increases.

The first evidence suggests that the in-depth concentration of the Au-NPs in the composite films is not homogeneous. Angle-resolved XPS (ARXPS[26]) analysis, reported in Figure 5, was performed in order to establish the occurrence of a nonisotropic in-depth particle distribution. As can be observed, the atomic percentages

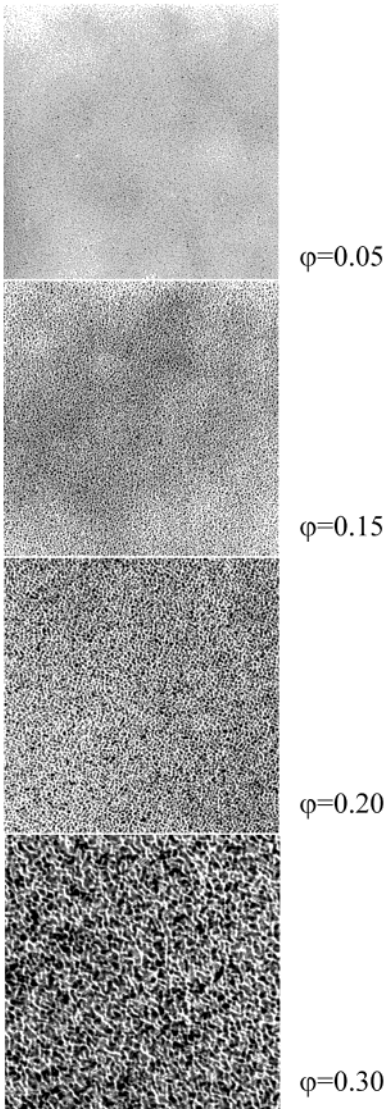

Figure 2. TEM photographs of CF_x(Au) nanocomposites having different gold contents, expressed as a volume fraction φ. Each photograph is relevant to a 500 nm × 500 nm area.

of carbon and fluorine are almost constant even when the sampled thickness is reduced to a quarter of its maximum. This indicates that the organic matrix, at least in the sampled layer, has a constant in-depth composition. Negligible fluorine surface segregation is observed as fluorinated long carbon chains are tied by a reticulated polymer structure, as will be proven later in the text. On the contrary, both gold and oxygen atomic percentages decrease as the sampled thickness decreases, that is as the outer surface is approached. Therefore, the in-depth dependence of the Au concentration confirms that the NPs are not homogeneously distributed in the material and their concentration decreases within the surface region. This nonisotropic distribution is most probably due to the fact that the ion-sputtered Au-NPs, being energetic clusters, easily penetrate the already deposited organic material. The lower oxygen atomic percentage in the outer layer can be explained assuming that oxygen is mainly bound to

(26) Dilks, A. In *Electron Spectroscopy, Theory, Techniques and Applications;* Brundle, C. R., Baker, A. D., Eds.; Academic Press: New York, New York, 1981; Vol. 4.

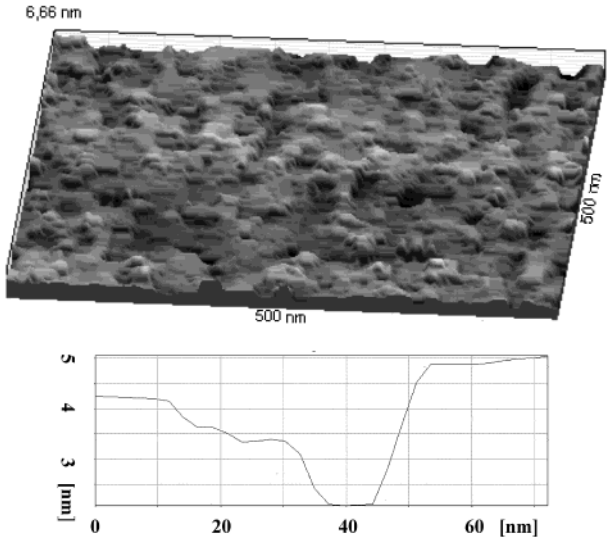

Figure 3. (a) 500 nm × 500 nm AFM image of the surface of a CF_x(Au) film ($\varphi = 0.15$). The white line indicates the site on which the profile reported in Figure 3b has been measured.

Table 2. Au-NPs Average Diameter and Surface Numeric Density Values Obtained from the TEM Images of Figure 2

φ	Au-NPs mean diameter (nm)	Au-NPs numeric density (Au-NPs × cm^{-2})
0.05	2.0 ± 0.6	$6.63 \times 10^{+12}$
0.15	2.7 ± 0.7	$4.98 \times 10^{+12}$
0.20	3.6 ± 1.5	$2.37 \times 10^{+12}$
0.30	7.8 ± 3.5	$7.7 \times 10^{+11}$

the Au-NPs, rather than being bound to the polymer matrix at the air-exposed surface; this hypothesis is also supported by evidence ii. Anyway, it should be kept in mind that, because of the extremely low oxygen percentages, the oxygen trend is affected by a not negligible error.

C 1s Region: Structure of the Fluoropolymer. Information on the structure of the organic matrix can be derived by the curve-fitting of the high-resolution C 1s region. As expected for a Teflon-like material, this region is quite complex; six peaks have been used to fit the signal, and a weak shoulder has been identified in the high binding energy region. Their attribution is reported in Figure 6, along with an overlay of C 1s spectra relevant to samples having $\varphi = 0-0.30$. Four peaks are unambiguously attributed to species that are typical of a Teflon-like matrix:[23,27] CF_3 (293.7 ± 0.1 eV), CF_2 (291.8 ± 0.1 eV), CF (289.8 ± 0.1 eV), and C−CF (286.9 ± 0.3 eV). An intermediate peak, falling at 288.5 ± 0.2 eV, could be attributed to both carbonyls (C=O) and fluorinated-unsaturated groups (C=CF).[26] Carbonyls are minor species, commonly present on the surface of air-exposed samples. However, since the oxygen surface percentage is always less than 1%, if the peak falling at 288.5 eV were exclusively due to C=O groups,[28] its intensity would be much lower, at most $^1/_4$ or $^1/_3$ of the measured value. Consequently, C=CF species are expected to give the main contribution to this signal. Their presence is confirmed by the weak shoulder (not fitted) centered at approximately 296 eV

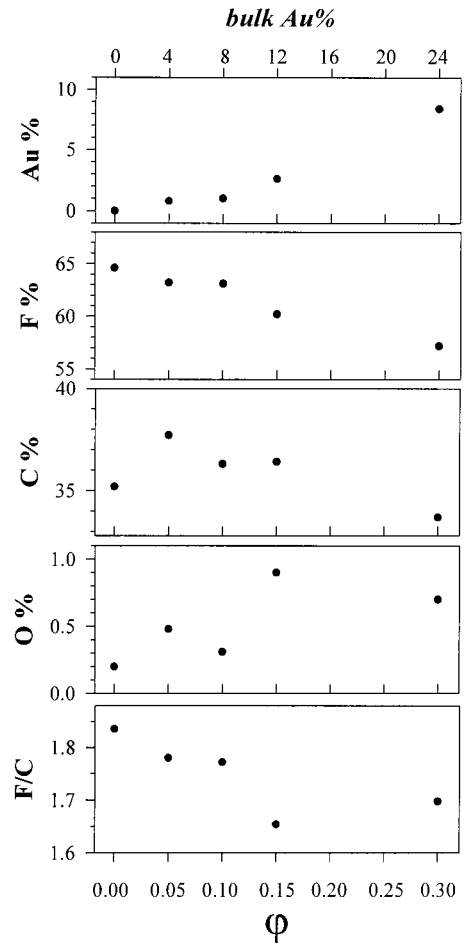

Figure 4. Dependence of the surface atomic percentages and fluorine/carbon ratio upon φ. To facilitate data interpretation, a second abscissa has been added on the top of the figure, reporting the bulk atomic gold percentages that correspond to the volume fractions φ.

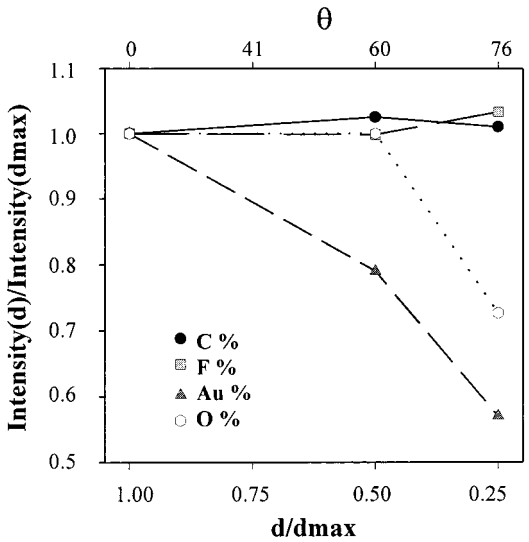

Figure 5. Angle-resolved XPS analysis of a CF_x(Au) film ($\varphi = 0.15$). The atomic percentages have been normalized by their value recorded at the take off angle $\theta = 0$, that corresponds to the maximum analyzed thickness "d_{max}". A double abscissa was used in order to allow an easier conversion between the take off angle and the sampled thickness.

(27) D'Agostino, R.; Cramarossa, F.; Fracassi, F.; Desimoni, E.; Sabbatini, L.; Zambonin, P. G.; Caporiccio, G. *Thin Solid Films* **1986**, *143*, 163.

(28) This is a deliberate overestimation that does not take into account the existence of gold oxides.

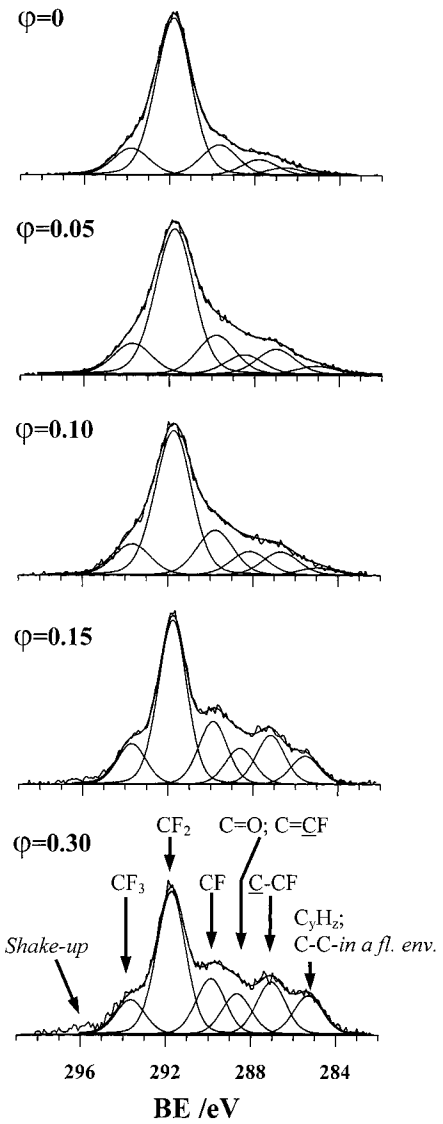

Figure 6. C 1s XPS spectra of CF_x(Au) films having different gold loadings. Experimental data are reported as solid lines, along with the curve-fit-originated peaks and their resultant.

and due to *shake-up* phenomena that are typical of unsaturated carbons.[26] Also the C 1s component falling at the lowest BE value (285.2 ± 0.3 eV) has a double nature. Carbons exclusively bound to other carbons in a fluorinated matrix, denoted as C−C-*in a fluorinated environment*[29] (BE > 285 eV[23,27]), are expected to contribute to this peak, along with hydrocarbon contaminants deriving from the vacuum system (C_yH_z species, BE = 284.8 eV). The binding energy and the intensity of this peak show a systematic increase with φ, different from what has been reported for plasma-deposited Teflon-like−gold composites.[15] In particular, in the $\varphi = 0-0.30$ range, the BE varies from 284.9 to 285.6 eV, suggesting that the contribution of the C_yH_z contaminant species dominates at low φ, while branched carbons-*in a fluorinated environment* dominate at high φ values. Moreover, the intensity increase of this peak indicates that the amount of the quaternary carbons in the material increases with increasing φ.

Quantitative data on the abundance of each different carbon species, derived from the results of Figure 6, are reported in Table 3. Gold inclusion causes the intensity of the peaks relevant to carbon species belonging to linear chains such as CF_2 (along with the CF_3 end groups) to decrease, while the intensities of tertiary and quaternary carbons (CF, C−CF, C−C-*in a fluorinated environment*), corresponding to branched structures, have the opposite trend. Also the "C=O; C=CF" peak increases with φ. As already discussed, C=O groups are less abundant than C=CF ones, and therefore unsaturated, fluorinated groups increase as the gold content is enhanced in the composite. This finding is also corroborated by the intensity trend of the *shake-up* shoulder falling at BE ≈ 296 eV.

The results of the C 1s curve-fitting can be used to evaluate polymer structural parameters such as the mean length of the linear segments of the chains (n) or the branching degree, expressed as total branched carbon percentage (C_{br}%). Quantitative treatment of fitting data is based on the following consideration: CF_2, C=O, and C=CF groups are the units composing the linear segments, while CF_3 and tertiary and quaternary carbons (CF, C−CF, C−C-*in a fluorinated environment*) terminate the linear segments. A linear segment can be described as follows:

$$-(CR_m)_n- \qquad \text{where } m = 1 \text{ when CR is C=O or C=CF and } m = 2 \text{ when } CR_2 \text{ is } CF_2$$

In Figure 7 values for n and C_{br}% derived from the data of Table 3 are reported as a function of φ. The data of Figure 7a are derived from eqs 1 and 2, reported in the inset of the figure; black circles are relevant to eq 1, while white squares have been obtained from eq 2. Equations 1 and 2 are based on the opposite assumptions that the peak falling at 285.2 eV is exclusively due either to carbons-*in a fluorinated environment* or to C_yH_z contamination, respectively. In a similar way, the polymer cross-linking extent has been calculated following the already mentioned assumptions of negligible (eq 3, black circles plot of Figure 7b) or total (eq 4, white squares plot of Figure 7b) contribution of hydrocarbons contamination to the peak falling at 285.2 eV. In Figure 7 data relevant to a Teflon standard have also been reported for comparison. Two important pieces of information can be derived from this figure. First, ion beam sputtering deposited CF_x films have shorter linear segments of chains and higher branching degrees than standard Teflon. This is an effect of the ion beam sputtering, that can be modulated by deposition parameters such as the energy of the Teflon target sputtering.[23] Second, a marked effect of the gold loading on the

Table 3. Quantitative Data Relevant to the C 1s Spectra of Figure 6 with Errors Derived from the Curve-Fit Procedure

φ	CF_3 %	CF_2 %	CF %	C=CF; C=O %	C−CF %	C−C, C_yH_z %
0	11.2 ± 0.6	65.5 ± 0.4	12.8 ± 0.6	6.6 ± 2.4	3.2 ± 2.3	0.8 ± 0.9
0.05	11.5 ± 0.5	54.5 ± 0.3	14.5 ± 0.7	7.2 ± 0.7	9.3 ± 0.5	3.0 ± 0.4
0.10	11.3 ± 1.0	52.8 ± 0.7	16.3 ± 1.0	8.6 ± 1.5	8.4 ± 0.8	2.6 ± 1.0
0.15	10.6 ± 0.3	43.2 ± 0.3	16.5 ± 0.7	9.4 ± 0.7	12.8 ± 0.5	7.4 ± 0.4
0.30	9.5 ± 0.3	39.1 ± 0.3	15.3 ± 0.5	11.1 ± 0.6	14.3 ± 0.3	10.6 ± 0.4

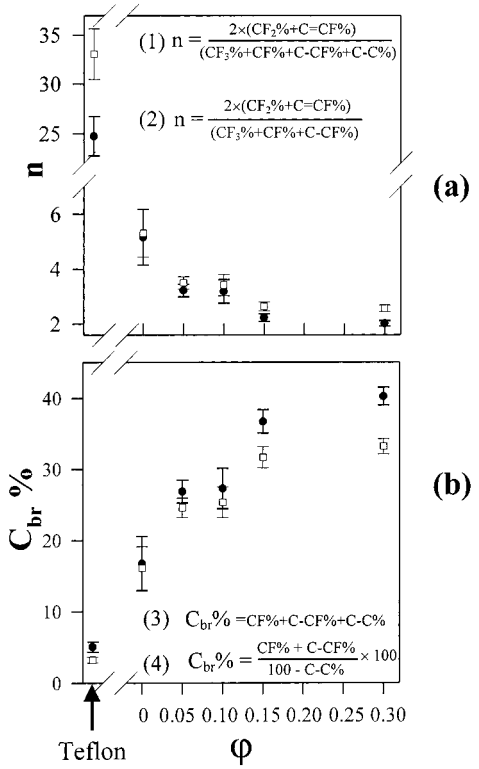

Figure 7. (a) Mean length of the linear segments of the fluoropolymer chains calculated by the data of Table 3 following the hypotheses of negligible (black circles) or total (white squares) C_yH_z contamination and using eq 1 or 2, respectively. (b) Branched carbon percentage over total C, calculated by the data of Table 3 following the already mentioned hypotheses of negligible (black circles) or total (white squares) C_yH_z contamination and using eq 3 or 4, respectively. In both parts of the figure, data relevant to a Teflon standard have been added for comparison. Error bars have been obtained by the propagation of the errors associated with the curve-fit peak percentages.

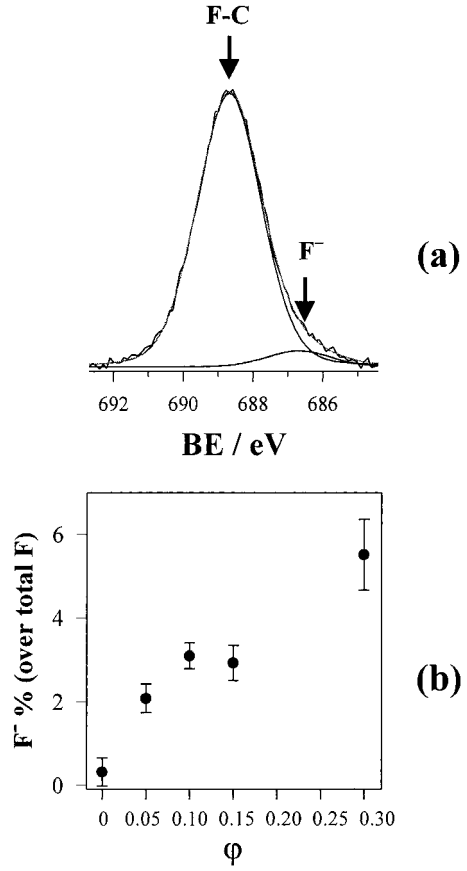

Figure 8. (a) F 1s XPS region of a CF_x(Au) film having a gold volume fraction of 0.30. Experimental data are reported as solid lines, along with the curve-fit-originated peaks and their resultant. (b) Dependence of the fluoride peak percentage (over the total F 1s signal) upon the gold loading in the composite.

fluoropolymer structure can be observed too; as a matter of fact *n* decreases and C_{br}% increases with φ.

Considering that the increase of gold loading is achieved by increasing the gold sputtering ion beam energy and current, it is plausible that the inclusion of higher amounts of energetic gold nanoparticles acts as an additional sputtering over the already deposited material, causing a cross-linking enhancement and shortening the length of the linear segments. Consequently, increasing values of φ lead to more tied and organized polymeric structures. It is also worth noting that the results discussed are independent of the assumptions made on the nature of the peak falling at 285.2 eV, since no different trends can be observed for *n* and C_{br}% if black circles or white squares are considered.

F 1s Region. High-resolution analysis of the F 1s region provides information on the composition of the interface between the Au-NPs and the polymer matrix. The curve-fitting of this region, reported in Figure 8a, has been carried out considering a main peak (BE = 688.7 ± 0.1 eV), due to polymer-bound fluorine, and a minor peak (BE = 686.4 ± 0.2 eV) due to a fluoride species. Since the fluoride content increases with φ (see Figure 8b), it is conceivable that gold fluoride species are present at the gold−polymer interface. Fluoride species have already been observed in an XPS study of gold thin films deposited by sputtering on Teflon-like materials, and they have already been attributed to gold fluorides whose stoichiometry has not yet been specified.[3]

Au 4f Region. An overlay of the Au 4f spectra relevant to composites having different gold volume fractions is reported in Figure 9. The peak parameters of the Au $4f_{7/2}$ main component are reported in Table 4, where they are compared with those relevant to a bulk Au sheet. As can be observed, the BE and HWHM values of the composites' Au 4f signal are systematically higher than those of bulk gold and show a marked shift toward higher values as φ decreases. A detailed discussion of this experimental evidence is reported in the following. Interestingly, this evidence can be partly ascribed to the presence of oxide and fluoride species. This is noteworthy, since gold oxide and fluorides are reactive species that are expected to play a crucial role in the gas-sensing mechanism.

Shape and Position of the Au 4f Signal. Due to the spin−orbit splitting, the Au 4f signal is a doublet, with the two components, Au $4f_{7/2}$ and Au $4f_{5/2}$, falling at low and high BE values, respectively. As can be observed in Figure 9, the BE values of the CF_x(Au) Au 4f spectra are systematically higher than those of bulk Au. More-

(29) Since there were no hydrogen sources in the deposition chamber, C−C-*in a fluorinated environment* species are quaternary carbons, contributing to the polymer branching.

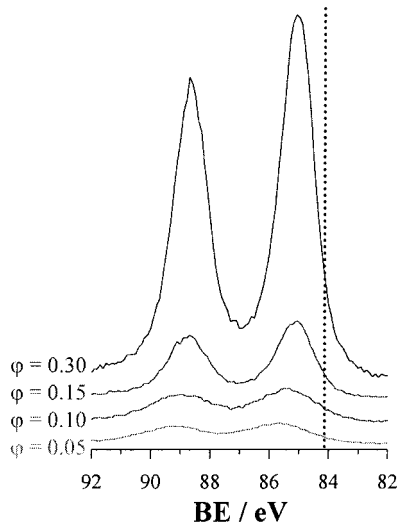

Figure 9. Overlay of Au 4f XPS regions relevant to composites having different gold loadings. The dotted line indicates the BE position of the Au $4f_{7/2}$ peak of a bulk Au standard.

Table 4. Experimental XPS Peak Parameters Relevant to the Au $4f_{7/2}$ Peak Component of CF_x(Au) Films and Bulk Au

φ	Au $4f_{7/2}$ BE (eV)	Au $4f_{7/2}$ HWHM (eV)
0.05	85.7	1.15
0.10	85.4	1.15
0.15	85.1	0.75
0.30	85.0	0.65
bulk Au	84.0	0.55

over Au-NPs' BEs and HWHMs show a marked shift toward higher values as φ decreases. Three different phenomena are expected to contribute to these trends.

First, it is well-known that the BEs and HWHMs of photoelectron signals generated by nanodispersed metals systematically increase as the average size of the clusters decreases.[30−33] This size effect has been attributed to the reduced ability of a small particle (with respect to a bulk material) to screen the final-state potential arisen in the core−hole after the photoionization process by means of the conduction electrons.[30,31] Final state charging effects have also been claimed by Di Cenzo et al.,[32] while Parmigiani et al., in their study on clusters deposited on insulating substrates, have hypothesized that surface tension of small spherical metal clusters deposited on Teflon matrixes may give rise to additional peak broadening and BE shifts.[33] Anyway, the amount of small-size-generated BE shifts reported for metallic Au nanoclusters having a diameter comparable to that of the Au-NPs of the present study is smaller than that reported in Table 4,[30] thus suggesting that other effects are also present.

A second phenomenon can generate HWHM and BE increases. Due to the presence in the samples of oxygen and fluoride, oxidized gold species are expected to be present on the surface of the clusters, along with metallic gold, thus broadening the convoluted peak and enhancing its BE.

As will be discussed below, at the present stage the effective amount of oxygen bound to gold and the stoichiometry of the gold fluorides are still unknown; however, indirect estimations allow us to state that at low φ values oxidized and metallic gold could have similar intensities, thus enlarging the resultant peak width and shifting its BE toward higher values.

Differential charging on insulating sample surfaces during XPS analysis is also known to give rise to peak broadening. In the case of CF_x(Au) films having lower conductivity values ($\varphi \leq 0.10$), this phenomenon certainly contributes to increase the Au 4f signal width. As a matter of fact, noticeable charging has been observed for these samples, and peak broadening has been evident in all their high-resolution XPS regions (compare, for instance, the HWHM of homologous C 1s peaks in Figure 6). Nevertheless, this third phenomenon does not exclude the other two. In fact, sample charging for $\varphi = 0.15$ and 0.30 was negligible and the HWHM values for C 1s and F 1s were not at all widened; this allowed us to exclude differential-charging broadening. Notwithstanding this, both the Au $4f_{7/2}$ BE and the HWHM decrease as the gold volume fraction increases from 0.15 to 0.30.

Consequently, all these phenomena can simultaneously influence the shape and position of the Au 4f signal, thus definitively complicating its curve-fitting.

Estimation of the Concentration of Au Oxide and Fluoride Species. Due to the reasons previously mentioned and to the lack of or the instability of appropriate nanodispersed standards, curve-fitting of the Au 4f region was not performed. Consequently, the precise amount of oxygen bound to gold[34] and the stoichiometry of the gold fluorides are still unknown. However, the concentrations of oxide and fluoride species have been indirectly estimated by the O 1s and F^- signals. Results are reported in Table 5, where a rough estimation of the Au_2O_3 content has been obtained using the difference between the intensity of the oxygen measured in the composites and that measured for CF_x ($\varphi = 0$). This quantification could also be affected by water adsorption, as reported in ref 35. In a similar indirect way, the amount of gold fluorides was obtained by the fluoride percentage calculated by curve-fitting of the F 1s spectrum.

CF_x(Au) Structure and Swelling Properties. On reviewing the reported results, we can assess that gold inclusion causes a progressive defluorination of the organic matrix, lowers the percentage of the groups associated with linear chains, and enhances that of tertiary, quaternary, and unsaturated fluorinated carbons. These structural changes can be reasonably explained as follows: sputter-deposited gold causes C−F bonds and C−C chains to break[2] in the organic matrix. The produced radicals can then react through rearrangement or recombination processes, leading to the already mentioned branched and unsaturated carbons.

(30) Oberli, L.; Monot, R.; Mathieu, H. J.; Landolt, D.; Buttet, J. *Surf. Sci.* **1981**, *106*, 301.
(31) Ascarelli, P.; Cini, M.; Missoni, G.; Nistic, N. *J. Phys. C2* **1977**, *38*, 125.
(32) Di Cenzo, S. B.; Wertheim, G. R. *Comments Solid State Phys.* **1985**, *11*, 203.
(33) Parmigiani, F.; Kay, E.; Bagus, P. S.; Nelin, C. J. *J. Electron Spectrosc. Relat. Phenom.* **1985**, *35*, 257.
(34) Due to the extremely low intensity of the O 1s signal, its curve-fit was not performed. A qualitative inspection of this spectral region reveals a noisy and broad line-shape with one or two unresolved peaks in the 530−534 eV BE range, that may include peaks due to C═O, Au_2O_3, and chemisorbed water.
(35) Linn, J. H.; Swartz, W. E. *Appl. Spectrosc.* **1985**, *39*, 755.

Table 5. Estimation of the Amount of Oxide and Fluoride Gold Species in the CF_x(Au) Nanocomposites with Two Possible Stoichiometries Hypothesized for the Gold Fluorides and Used for the Estimation of the Total Oxidized Gold Percentage

φ	Au_2O_3 % = 0.67(O $\%_{CF_x(Au)}$ − O $\%_{CF_x}$)	AuF_5 % = 0.2(F^- %)	AuF_3 % = 0.33(F^- %)	Au oxide + fluoride % estimated	total Au % measured
0.05	0.2	0.3	0.4	0.5−0.6	0.8
0.10	0.1	0.4	0.7	0.5−0.8	1.0
0.15	0.5	0.4	0.6	0.9−1.1	2.6
0.30	0.3	0.6	1.0	0.9−1.3	8.4

Branched chains could also be produced by the so-called "Toy process",[36] that exploits the catalytic effects of metal fluorides and leads to the cross-linking reaction of unsaturated species. Gold effects have also been qualitatively observed in the XPS studies of plasma-deposited Teflon-like−gold composites[15] and of sputter-deposited gold thin films on Teflon-like materials.[3] In the present study, the use for the first time of curve-fitting procedures on CF_x(Au) nanocomposites allowed us to observe the presence of unsaturated groups and the dependence of their concentration on the gold loading. Quantitative information was also obtained on the increase of the percentage of branched groups and on the decrease of the mean length of the linear chain fractions, both by a factor of almost 3 in the $\varphi = 0-0.30$ range.

Moreover, due to the presence of fluorides and oxygen in the samples and also considering the already mentioned relationship between oxygen and gold signals, the interface between Au-NPs and the polymer is expected to be constituted of polar and reactive species such as gold oxides and fluorides, although unambiguous determination of their abundance through the curve-fitting of the Au 4f signal is not yet possible. The interface area, enriched by these species, could play a key role in the gas-sensing processes. For instance, electron-poor gold (Au^{ox}) could interact with polar molecules such as acetone,[20−21] leading to partial analyte−Au^{ox} coordination and enhancing the natural tendency of Teflon-like materials to undergo swelling.[37] This is also corroborated by the observation that the degree of swelling is an increasing function of the strength of the analyte molecule dipole moment. Another possible alternative or complementary mechanism could be based on the direct interaction between the fluoropolymer and the analyte through van der Waals interactions or charge transfers.[37] XPS and swelling studies on CF_x ($\varphi = 0$) films having the same branching degree as those of the present study will allow us to discriminate between different interactions. Moreover, since purely entropic effects are also expected to contribute to the swelling process, the application of thermodynamic models to this kind of study is presently under investigation.

(36) Toy, M. S. *J. Polym. Sci. Part C* **1971**, *34*, 273.
(37) Butler, M. A.; Buss, R. J.; Seager, C. H. *Appl. Phys. Lett.* **1991**, *59*, 2817.

Conclusions

A systematic study of the morphology and chemical structure of CF_x(Au) composites useful as active layers in gas-sensing devices has been presented. TEM analysis showed that the Au-NPs have an homogeneous in-plane distribution, while angle-resolved XPS indicated that their in-depth concentration is lower on the surface. XPS was used to study the structure of the organic matrix and its dependence upon the gold loading. The results indicate that the extent of cross-linking increases as the gold content increases, thus leading to a more tied and organized polymer structure. Moreover, XPS analysis showed that the interface between the organic matrix and the gold nanoparticles is composed of gold fluoride and oxide species. These polar and reactive species are expected to play a major role in the gas-sensing swelling phenomena that occur when the material is exposed to a polar solvent.

Acknowledgment. Dr. G. Bruno and Dr. M. Losurdo are gratefully acknowledged for the AFM measurements. Mr. A. Tambone and Mr. S. Giacummo are gratefully thanked for their skilled assistance during the XPS analyses. Mr. G. Casamassima is also gratefully thanked for technical support during the film depositions. This work was carried out with the financial support of C.N.R. and M.U.R.S.T.

CM0111940